A super-efficient and biosafe hemostatic cotton gauze with controlled balance of hydrophilicity/hydrophobicity and tissue adhesiveness

Huaying He[1#], Weikang Zhou[1#ξ], Jing Gao[1], Fan Wang[2], Shaobing Wang[2], Yan Fang[1*], Yang Gao[1], Wei Chen[1]*, Wen Zhang[1], Yunxiang Weng[1], Zhengchao Wang[2], Haiqing Liu[1,3*]

[1]College of Chemistry and Materials Science, Fujian Provincial Key Laboratory of Polymer Materials, Fujian Normal University, Fujian 350007, China

[2]Provincial University Key Laboratory of Sport and Health Science, College of Life Sciences, Fujian Normal University, Fuzhou 350007, China.

[3]Engineering Research Center of Industrial Biocatalysis, Fujian Province Higher Education Institutes, Fujian 350007, China

[#]These authors made equal contribution

[ξ] Current address: Zijin Middle School, Shanghang 364214, China

[*]Correspondence to: Haiqing Liu (E-mail: haiqingliu@fjnu.edu.cn)

Yan Fang (E-mail: fangyan_YWJ@163.com)

Wei Chen (Email: chenwei@fjnu.edu.cn)

Content

1. Synthesis of ABO and USO-g-gauze

(1) Synthesis scheme of ABO and ^{1}H-NMR

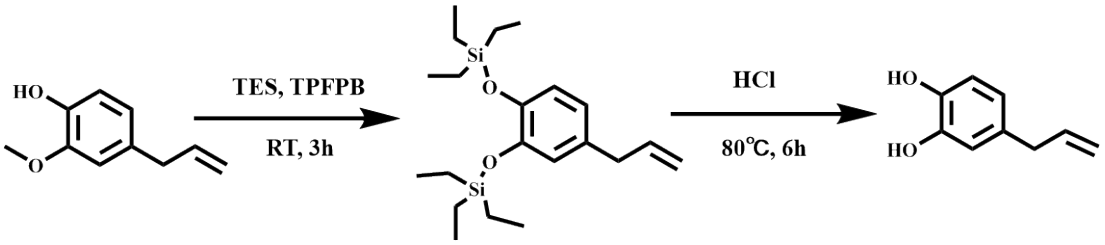

Scheme S1 Preparation scheme of 4-allyl-1, 2-benzenediol (ABO).

^{1}H-NMR of TES protected eugenol：6.78 ppm (d, 1H, Ar-*H*), 6.69 ppm (s, 1H, Ar-*H*), 6.63 ppm (d, 1H, Ar-*H*), 5.98 ppm (m, 1H, -C*H*=CH_2), 5.06 ppm (m, 2H, -CH=CH_2), 3.34 ppm (d, 2H, -CH_2-CH=CH_2), 0.98 ppm (t, 18H, -Si-CH_2-CH_3), 0.73 ppm (q, 12H, -Si-CH_2-CH_3).

^{1}H-NMR of ABO：6.78 ppm (d, 1H, Ar-*H*), 6.71 ppm (d, 1H, Ar-*H*), 6.62 ppm (dd, 1H, Ar-*H*), 5.93 ppm (m, 1H, -C*H*=CH_2), 5.29 ppm (b.s., 1H, -O*H*); 5.21 ppm (b.s., 1H, -O*H*), 5.05 ppm (m, 2H, -CH=CH_2), 3.27 ppm (d, 2H, -CH_2-CH=CH_2).

(2) Optimization of synthetic conditions for USO-g-gauze

Preliminary experiments to optimize the synthesis conditions were conducted. As listed in Table S1, four USO/ethanol solutions with USO concentration of 0.5, 1.0, 2.0 and 2.5% were used to make USO-g-gauze. The graft amount was ranged from 0.02 wt% to 0.28 wt% increasing with USO concentration. Water droplet instantly permeates and spreads in #1 and #2 gauzes, while it steadily stands on #4 within 60 s with WCA of ca. 120 (Fig. S1). #3 gauze has a unique wetting property, as detailed in our manuscript. In a pre-evaluation of their hemostatic ability in the rat femoral artery injury model, the hemostatic performance of #1 and #2 gauze is similar to that of standard cotton gauze, while #4 gauze is similar to HTMS-g-gauze. Therefore, #3 USO-g-gauze was prepared and used for the systematic study shown in the manuscript.

Table S1 WCA of a series of USO-g-gauze

USO-g-gauze	USO conc. in USO/ethanol solution (wt%)	Graft amount by weight (wt%)	WCA (°) at time of	
			0 s	60 s
#1	0.5	0.02	0	0
#2	1.0	0.04	0	0
#3	2.0	0.10	68.2 ± 2.1	0
#4	2.5	0.28	120.5 ± 3.5	120.2 ± 3.3

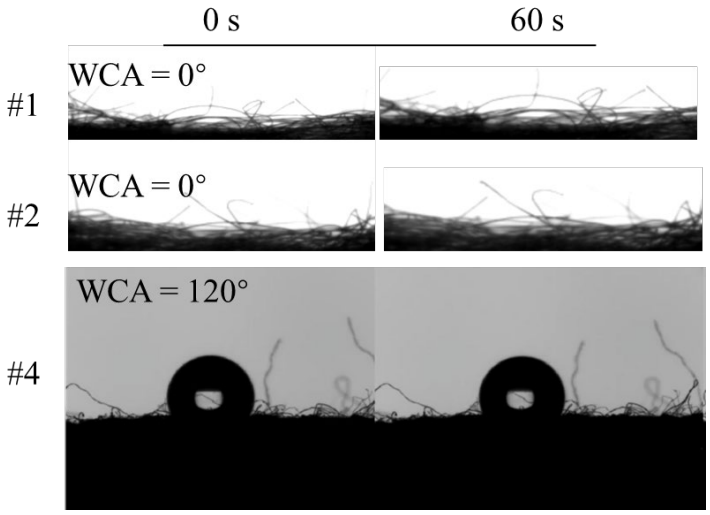

Fig. S1 WCA of #1, #2, #4 USO-g-gauze at 0 s and 60 s.

2. FTIR spectra of gauze samples

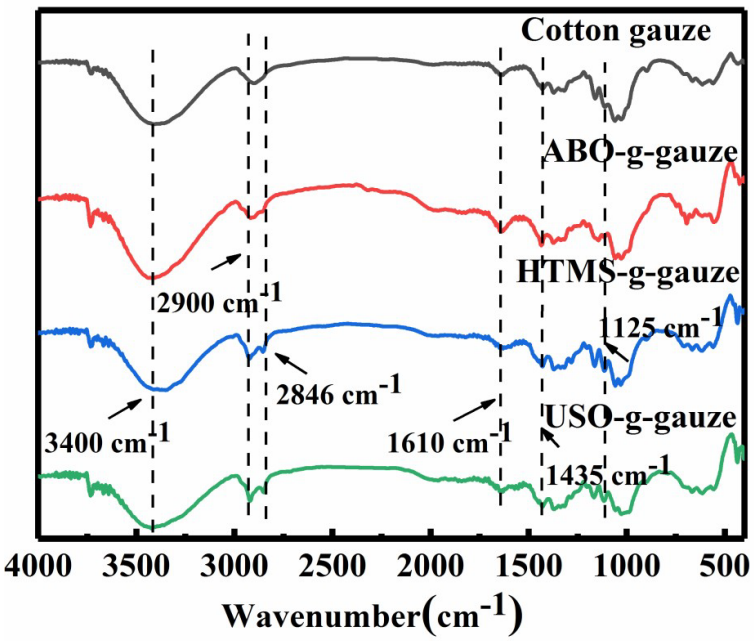

Fig. S2 FTIR spectra of gauze samples.

3. XPS analysis of gauze samples

XPS spectra of cotton gauze and USO-g-gauze are shown in Fig. S3. In the survey scan spectrum of the gauze, there are two distinct peaks of C_{1s} (286.40 eV) and O_{1s} (532.40 eV). An additional peak for N_{1s} (400.08 eV) is shown for USO-g-gauze (Fig. S3a). It is introduced by the low temperature plasma treatment in N_2 atmosphere.[1]

Based on the C1s high-resolution scan spectra (Fig. S3b), the C/O ratio of cotton gauze and USO-g-gauze is 1.9:1 and 2.5:1, respectively. The increasing C/O ratio of USO-g-gauze is due to that the grafted USO contains an alkyl chain with 15 carbons. The C1s signal is fitted into three categories, i.e. the three peaks at 284.96, 286.75, and 288.0 eV are respectively attributed to the carbon of C-C, C-O-H, and O-C-O/C=O bond of cellulose. For USO-g-gauze, the C1s peaks for C-C, C-O-H, and O-C-O/C=O bond appear at very similar locations: 284.68, 286.46, and 288.23 eV, respectively. However, the relatively strongest peak of USO-g-gauze is C-C bond, rather than that of cotton is C-O-/C-OH bond. This is in accordance with the abundance of C-C bond from the long aliphatic chain grafted on USO-g-gauze.

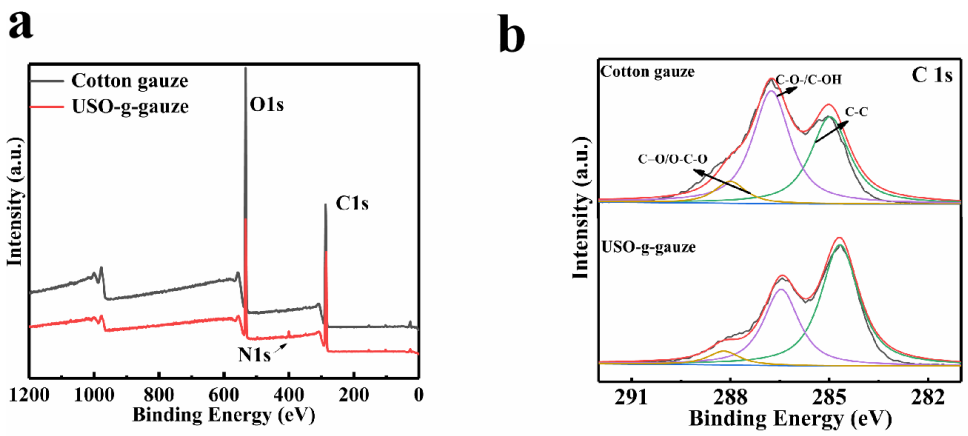

Fig. S3 (a) XPS survey and (b) C1s high resolution scan spectra of cotton gauze and USO-g-gauze.

4. SEM of gauze samples

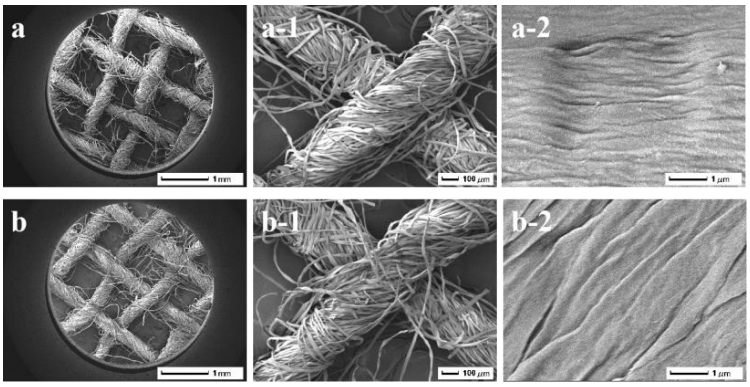

Fig. S4 SEM images of (a) ABO-g-gauze and (b) HTMS-g-gauze at different magnifications.

5. Hemostatic performance of USO grafted chitosan gauze (USO-g-chitosan)

(1) Preparation of USO-g-chitosan

A swatch of chitosan nonwoven was soaked in aq. acetic acid solution (pH 5.5) for 15 min, then put in 0.1 wt% sodium alginate (SA) aq. solution for 30 min at room temperature. Subsequently, the swatch was taken out and washed away free SA with distilled water, and completely dried at 60 °C. Then USO was grafted onto it through the same procedure for USO-g-gauze.

(2) Hemostatic performance on rat femoral artery injury

Chitosan nonwoven (Fig. S5A) (thickness: ca. 2 mm) was composed of microfibers with diameter of ca. 20 μm (Fig. S5B). Its chemical structure features -NH_2 groups in the anhydroglucose repeating unit, and it is a good source for efficient hemostatic products.[2, 3] USO was grafted onto chitosan fibers (Fig. S5C). Two gauze swatches stacked layer by layer (Fig. S5D) were compressed onto the transected rat femoral artery (Fig. S5E and F) for 5 sec, followed by static covering for a total time of 180 s (Fig. S5G and H). The gauzes were then removed to check the injuries (Fig. S5I and J). It is seen that re-bleeding occurs for the injury treated with chitosan gauze (Fig. S5K,

pointed by the yellow arrow), all four sides of the two swatches were blood-wetted because of blood absorption and diffusion (Fig. S5M), while the injury treated with USO-g-gauze is relatively clean (Fig. S5J and L) and only a small area on the first side was wetted with blood, even without diffusion to the second side (Fig. S5N). The blood loss for USO-g-chitosan is just 5.7% of that for chitosan gauze (Fig. S5O). The hemostatic efficiency of USO-g-chitosan was well demonstrated in Suppl. Video 4.

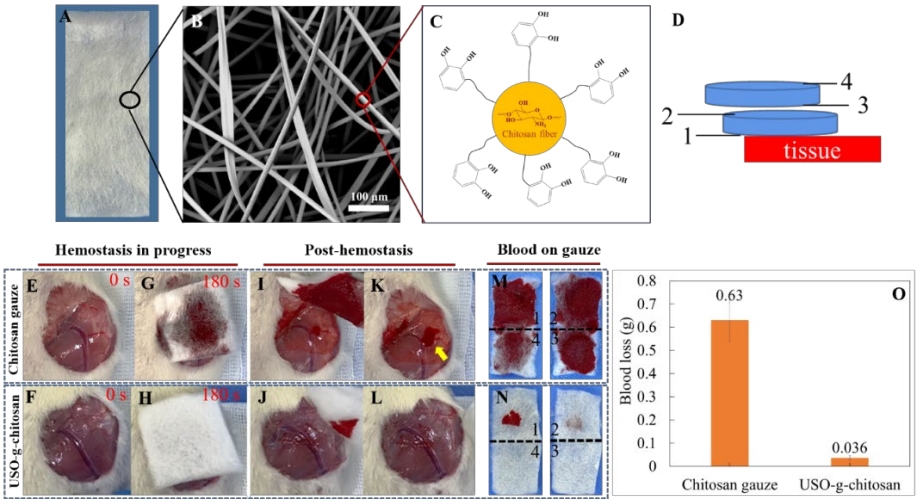

Fig. S5 (A) a digital photo and (B) a SEM image of USO-g-chitosan nonwoven gauze, (C) a cartoon for the chemical structure of USO-g-chitosan, (D) a cartoon for applying two gauze swatches stacked layer by layer on the bleeding tissue, the numbers indicate the side of the gauze, (E, F) rat femoral artery, (G) chitosan gauze and (H) USO-g-gauze on a bleeding artery for 180 s, (I-L) gauzes were removed after hemostasis to check the wounds, (M, N) blood absorption and diffusion in gauzes, the numerical number indicates the gauze side as shown in D, (O) blood loss for chitosan and USO-g-chitosan gauze.

6. Rat survival rate in the injury models

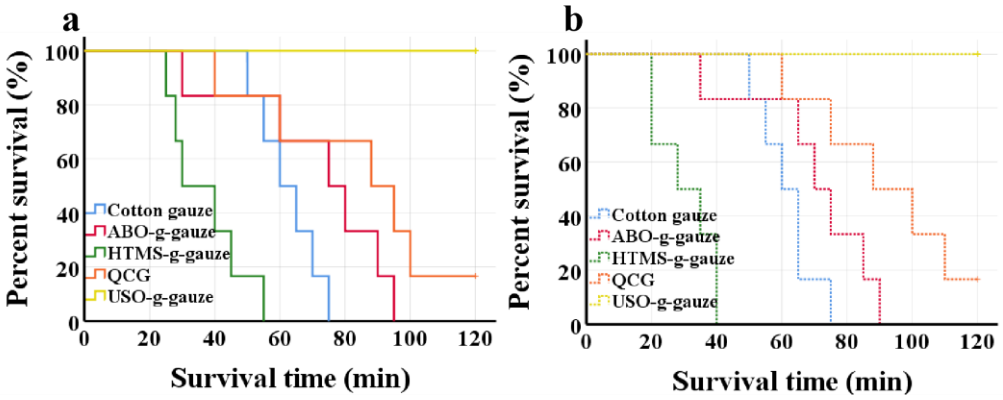

Fig. S6 Survival rates in the rat (a) femoral artery injury and (b) liver injury models treated with gauzes.

7. Hemostasis in the pig skin laceration model

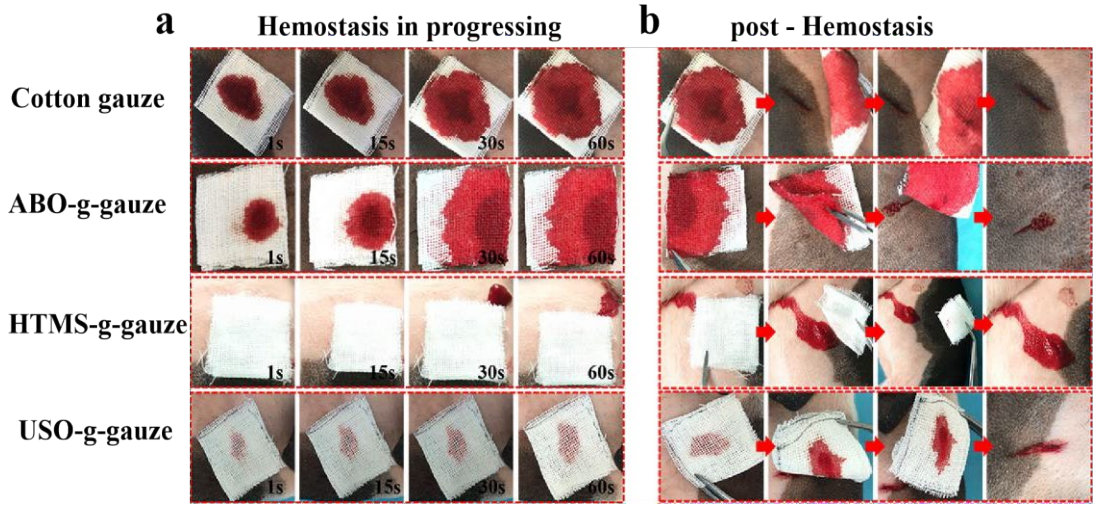

Fig. S7 Hemostasis in the pig skin laceration model. (a) Progressing of hemostasis after gauzes were put on wound, and (b) Removing gauze from wound after hemostatic state was reached.

8. Theoretical insight into the excellent tissue adhesiveness of USO-g-gauze

The generalized gradient approximation (GGA) with the Perdew–Burke–Ernzerh (PBE)[4] of the exchange correlation functional (including a semi-empirical van der Waals (vdW)[5] correction to account for the dispersion interactions) and a 400 eV cutoff

for the plane-wave basis set are adopted to perform all the density functional theory (DFT)[6] computations of the studied systems within the frame of the Vienna ab initio simulation package (VASP)[7, 8]. The projector-augmented plane wave (PAW) is used to describe the electron-ion interactions[9, 10]. The atomic relaxation is performed until the total energy variation is smaller than 10^{-4} eV and all forces on each atom are 0.02 eV $Å^{-1}$.

Moreover, the following equation is defined to calculate the adsorption energies of the amino acid molecules on the modified cellulose with the alkyl chain terminated with catechol:

$$\Delta E_{ads} = E_A + E_B - E_{AB} \quad (1)$$

Where E_A, E_B and E_{AB} are the total energies of the alkyl-chain-modified cellulose, the sole amino acid molecule, and the composite system, respectively.

Initially, the geometric structure of cellulose has been fully optimized, as show in Fig. S8a. Its optimized lattice parameters are a = 7.72, b = 8.45 and c = 21.97Å, respectively, all of which are close to the corresponding experimental results[11]. Subsequently, we construct the structural model of composite system, namely the modified cellulose structure with the alkyl chain containing fifteen carbon atoms in the skeleton and having the terminal linked with catechol. Specifically, based on the optimized cellulose structure, we employ the structural unit as the theoretical model to simulate the structure of cellulose, and then connect the optimized alkyl chain to the surface of cellulose by substituting the H atom of the hydroxyl group, as illustrated in Fig. S8b. We have fully optimized the structure of this model, and named it CAC for convenience. Meanwhile, we also optimized 16 different kinds of amino acid molecules (Figs. S8c and S8d), which can be used as important components of the peptide chain in the protein, including alanine (A), asparticacid (D), glutamicacid (E), phenylalanine

(F), glycine (G), isoleucine (I), lysine (K),leucine (L), methionine (M), asparagine(N), glutamine (Q), arginine (R), serine (S), threonine (T), valine (V) and tyrosine (Y).

Ultimately, based on the structural model of CAC, we carried out the DFT calculations to investigate the adsorption properties of the alkyl-chain-modified cellulose system for the correlative amino acid molecules, by considering the possible adsorption configurations. We calculated the adsorption energies (ΔE_{ads}) of amino acid molecules on the CAC system by the formula (1), where the possible interaction modes were considered, such as the π-π stacking interaction and hydrogen bond interaction.

After relaxation, we can find that the amino acid molecules Y and F with the benzene ring can ultimately be adsorbed on the catechol at the end of alkyl chain via the π-π stacking interaction with the distance between two rings as 3.424 Å and 3.408 Å respectively, as shown in Fig. 1c and Table S2. At the same time, the hydrogen bonding interaction can be also observed between them, where the H atom in a OH group of catechol can effectively interact with the lone pair of N atom in NH_2 group in amino acid molecule Y or F, with the interaction distance about 1.720 Å, as illustrated in Fig. S8c. All of these can be also supported by the distribution of the correlative electron densities and the calculated electrostatic potentials (Fig. S8c). As a result, the computed ΔE_{ads} values for F and Y are as large as 0.621 and 0.729 eV (Fig. S8c), respectively, indicating that these two amino acid molecules containing the π-conjugated-ring can be effectively adsorbed on the catechol of CAC structure through the synergistic action of π-π stacking and hydrogen bonding.

Comparatively, all the remaining fourteen amino acid molecules, including A, D, E, G, I, K, L, M, N, Q, R, S, T and V, can effectively interact with the catechol of CAC structure by adopting two hydrogen bonds. It can be found that one hydrogen bond is formed by the H atom in COOH group of correlative amino acid molecules interacting

with O in one OH group of catechol, while another hydrogen bond is formed through the O atom in COOH group interacting with H in another OH group of catechol, as presented in Fig. S8d. This can be also supported by the calculated electrostatic potentials (Fig. S8d). All these hydrogen bonding distances are in the range of 1.69 ~ 1.80 Å (Table S2), and the computed ΔE_{ads} values are as large as 0.598, 0.622, 0.639, 0.617, 0.637, 0.637, 0.570, 0.636, 0.619, 0.637, 0.602, 0.592, 0.603 and 0.607eV for A, D, E, G, I, K, L, M, N, Q, R, S, T and V, respectively (Fig. S8d), indicating the strong interaction between them.

Furthermore, we also explore the effect of relative position between two OH groups on the benzene ring on the adsorption energy of the sampled amino acid molecule G on the modified cellulose system, by considering three different configurations I~III, in which the two OH groups are separated by one, two or three H atoms, respectively, as shown in Fig. S9. Our computed results reveal that when changing the relative position between the two OH groups from the original ortho- to meta- to para-arrangements, the ΔE_{ads} values for G can be reduced from 0.617 to 0.502/0.419 and then to 0.397/0.384 eV. Further, when the two OH groups are separated by three H atoms, the small adsorption energy (*ca.* 0.383/0.355eV) can be maintained. Clearly, with the increase of the spacing distance between the two OH groups, the adsorption energy for the sampled amino acid molecule decreases significantly, in view of the fact that two hydrogen bonds cannot be effectively formed at the same time or only single hydrogen bond can be formed (Fig. S9). Therefore, the relative position between two OH groups on the benzene ring can have an important influence on the adsorption energy, where the ortho position can bring the maximum adsorption energy due to the formation of two hydrogen bonds.

Further, we also calculated the adsorption energy ΔE_{ads} of the sampled amino acid

molecule G on the modified cellulose system with the alkyl chain terminated by phenol with one OH group, which can be considered as the corresponding structure by removing one of two OH groups in catechol of CAC. As shown in Fig. S10, two configurations I and II can be obtained, where single hydrogen bond is observed between G and phenol with a distance about 1.804 and 1.753 Å, respectively. The computed ΔE_{ads} values are 0.248 and 0.355 eV, respectively, both of which can be about half of that of the corresponding structure with the two hydrogen bonds. This means that both the hydrogen bonds can be effectively formed simultaneously between the relevant amino acids and catechol in CAC. Clearly, all of these can reflect the superior structural match between the amino acid molecules and the catechol used.

Overall, the modified cellulose structure with the alkyl chain can effectively interact with all these amino acid molecules via two hydrogen bonds or the synergistic action of π-π stacking and hydrogen bonding, indicating that this new type of hemostatic cotton fabric can exhibit excellent issue adhesiveness, where the catechol at the end of alkyl chain can play a crucial role.

Table S2. The computed bond lengths ($d_{H\text{-}O}$) of the related hydrogen bonds as well as the distance ($d_{\pi\text{-}\pi}$) between two parallel benzene rings for all sixteen optimized structures CAC-X with CAC interacting with different amino acid molecules X

CAC-X systems	Bond lengths (Å)	
X=	$d_{H1\text{-}O1}$	$d_{H2\text{-}O2}$
A	1.765	1.706
D	1.783	1.712
E	1.771	1.728
G	1.754	1.719
I	1.770	1.704
K	1.776	1.697
L	1.717	1.712

M	1.725	1.725
N	1.740	1.706
Q	1.804	1.700
R	1.804	1.728
S	1.773	1.702
T	1.771	1.677
V	1.761	1.708
		$d_{\pi\text{-}\pi}$
F		3.424
Y		3.408

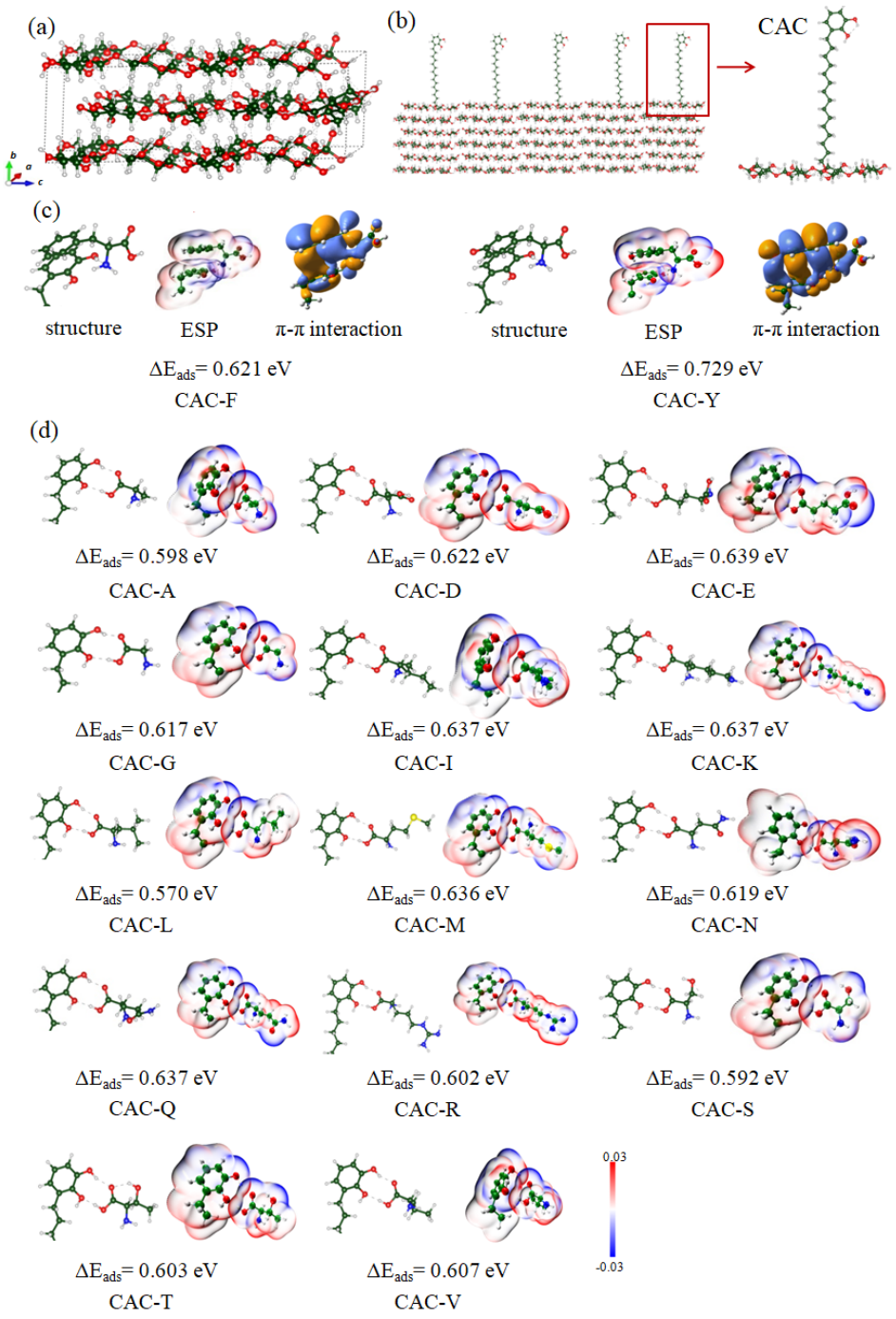

Fig. S8. (a) Bulk structure of cellulose. (b) The structural model of modified cellulose structure with the alkyl chain containing fifteen carbon atoms in the skeleton and having the terminal linked with catechol. (c) Two optimized structures CAC-X (X= F and Y) with USO-g-gauze interacting with the amino acids X containing benzene ring and the corresponding adsorption energies (ΔE_{ads}) as well as the electrostatic potentials and the correlative electron densities, where only the upper part of the structure is provided for clarity. (d) The remaining fourteen optimized structures CAC-X with CAC interacting with different amino acid molecules X, as well as the corresponding adsorption energies (ΔE_{ads}) and the electrostatic potentials. The dark green, white, blue, red and yellow balls represent C, H, N, O and S atoms, respectively.

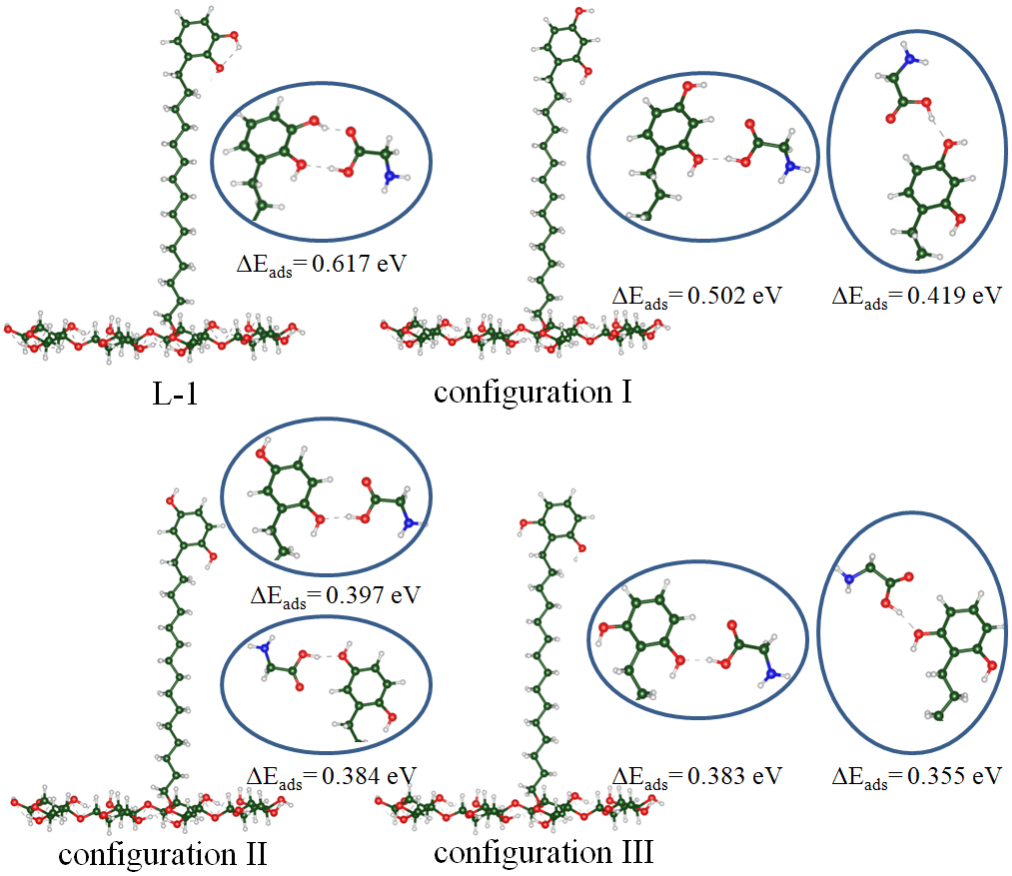

Fig. S9. The effect of relative position between two OH groups on the benzene ring on the adsorption energy by sampling amino acid molecule G interacting with the modified cellulose system.

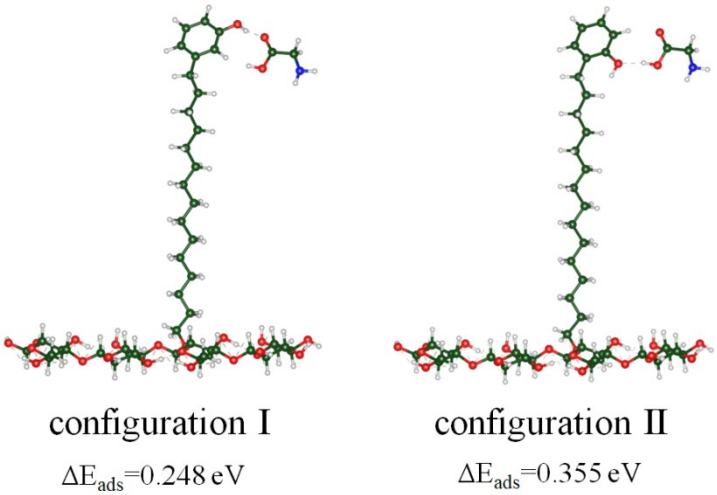

Fig. S10. The two correlative configurations for adsorbing the sampled amino acid molecule G on the modified cellulose system with the alkyl chain terminated by phenol with one OH group, and the corresponding adsorption energies.

9. Peeling force of gauze on the fresh wet rat femoral tissue

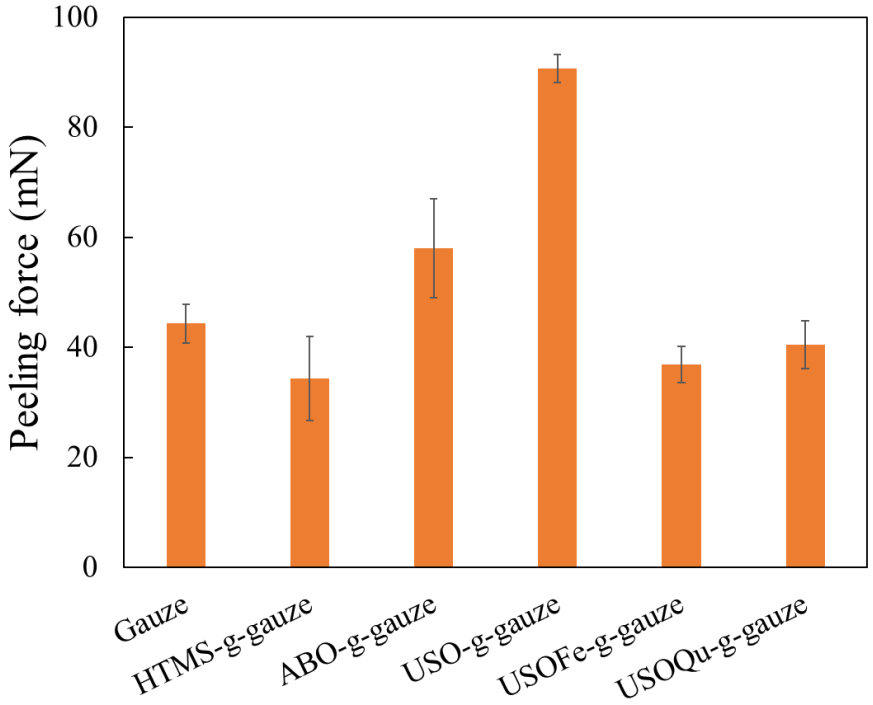

Fig. S11 Peeling force of gauzes on the rat femoral tissue

10. Inactivation of catechol groups on USO-g-gauze and their hemostatic performance

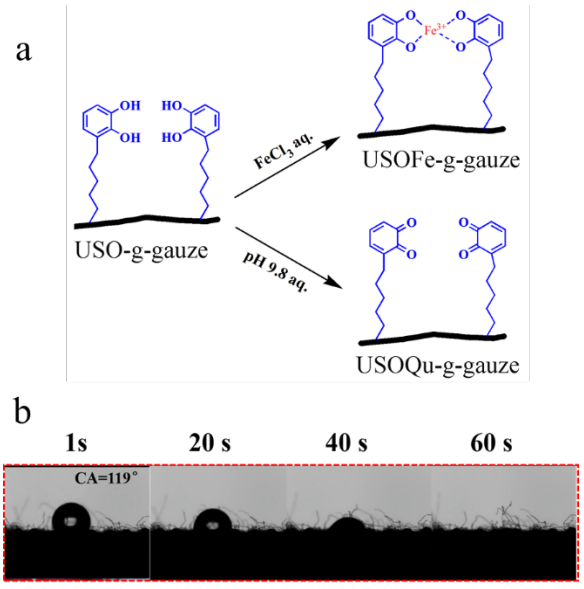

Fig. S12 (a) Schematic diagram of the chelation reaction between catechol groups and Fe^{3+} in the USOFe-g-gauze, and the transformation of catechol to quinone in pH 9.8 aq. solution for USOQu-g-gauze. (b) Water contact angle of USOFe-g-gauze with time.

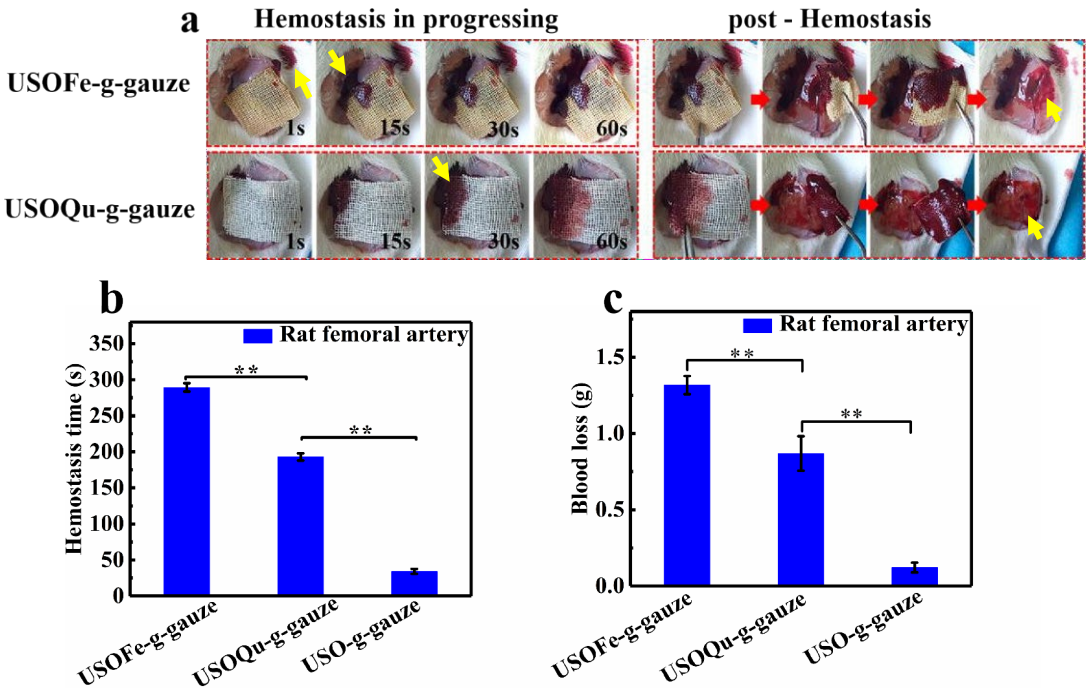

Fig. S13 (a) Gauze was put on the bleeding rat femoral artery injury, then it was removed from the wound after hemostatic state was reached. (b) Hemostatic time and (c) blood loss in the rat femoral artery injury model.

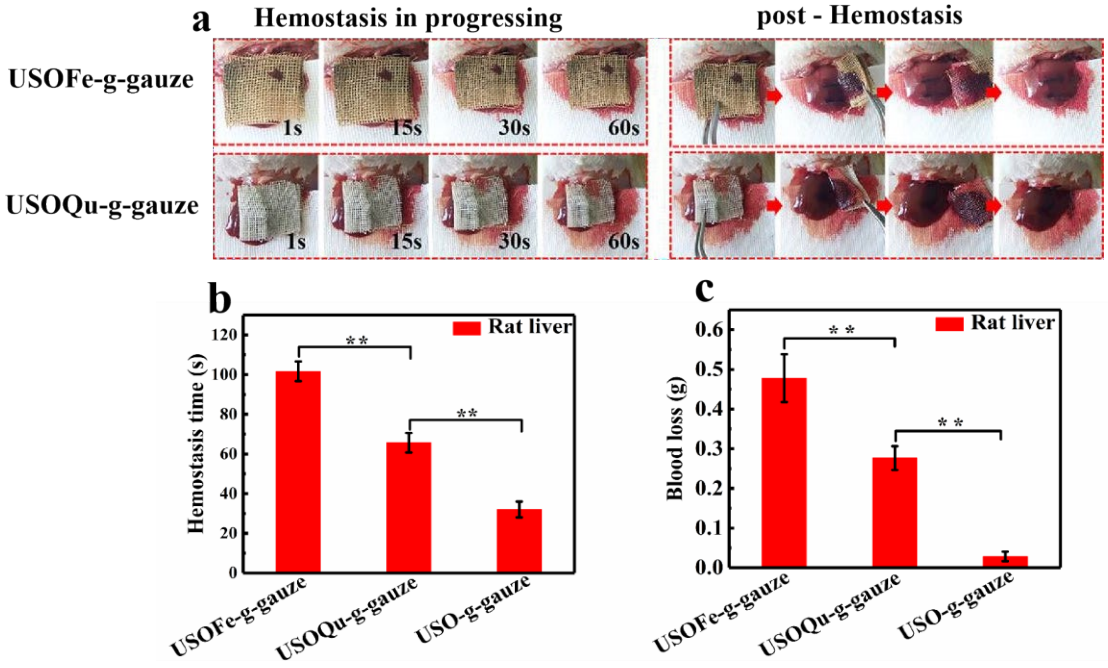

Fig. S14 (a) Gauze was put on the bleeding rat liver injury, then it was removed from the wound after hemostatic state was reached. (b) Hemostatic time and (c) blood loss in the liver injury models.

11. Morphology of Bandage®

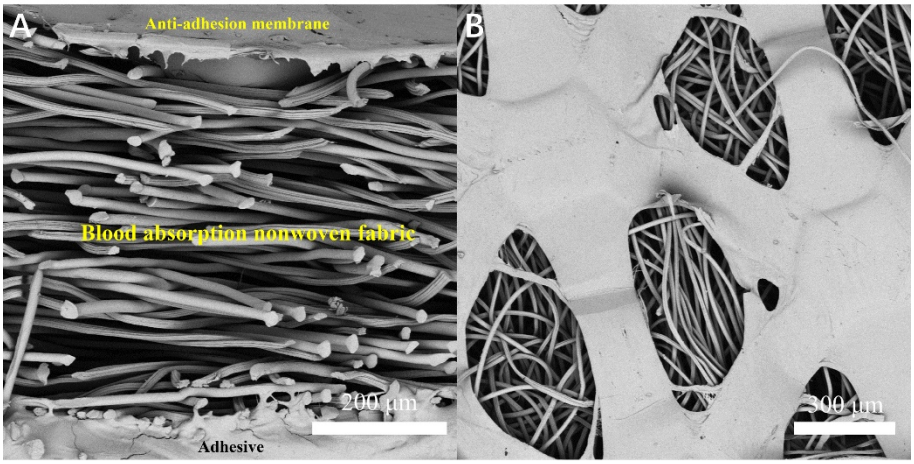

Fig. S15 SEM images of (A) cross-section and (B) topology of a bandage

12. Growth and proliferation of L929 on gauze samples

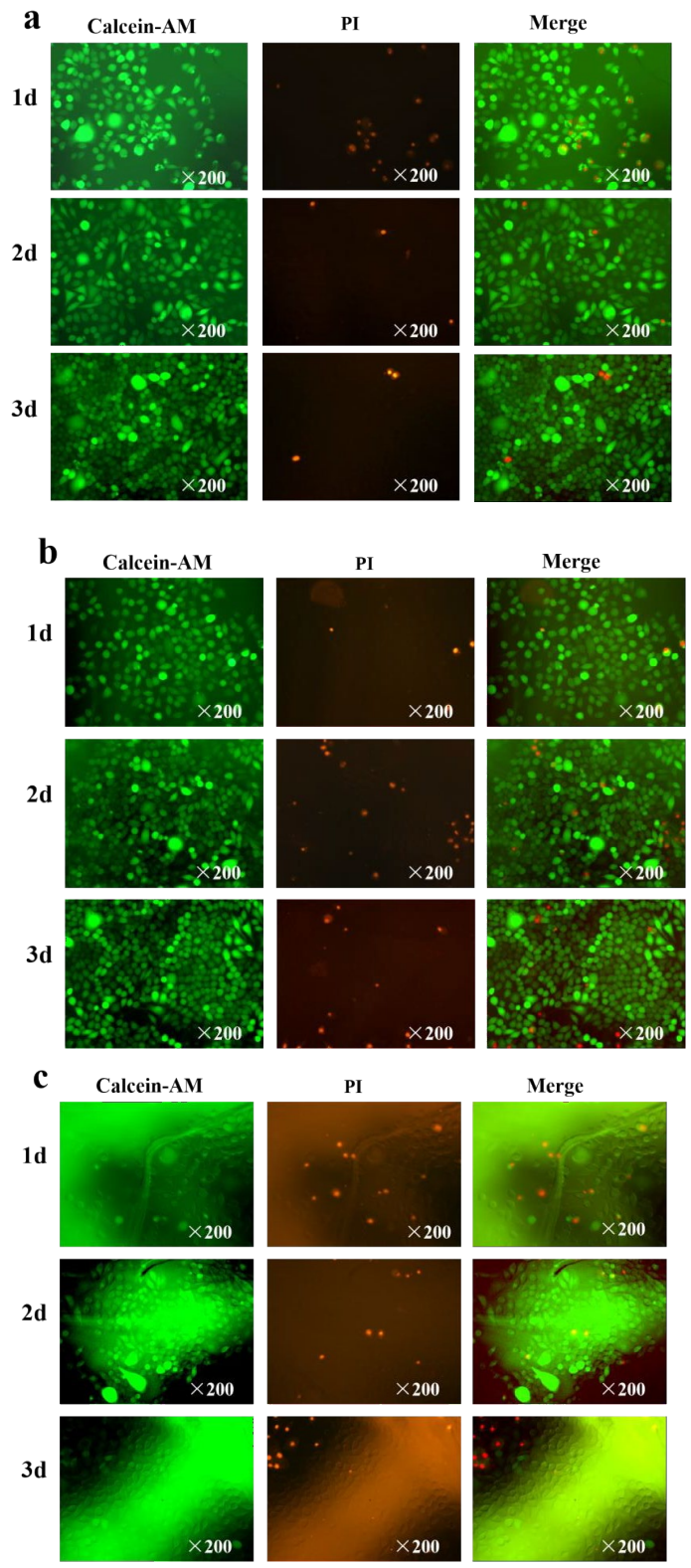

Fig. S16 Optical microscopy images of L929 cells incubation on (a) cotton gauze, (b) ABO-g-gauze, and (c) HTMS-g-gauze for 1, 2, and 3 d.

13. List of videos

Video S1. Water absorption dynamic of gauzes.

Video S2. Non-compressing hemostasis by gauzes in rat femoral artery injury model.

Video S3. Compressing-hemostasis by HTMS-g-gauze and USO-g-gauze in rat femoral artery injury model

Video S4. Compressing-hemostasis by chitosan and USO-g-chitosan gauzes in rat femoral artery injury model.

Video S5. Non-compressing hemostasis in rat liver injury model.

Video S6. Hemostasis by cotton gauze in pig femoral vein injury model.

Video S7. Hemostasis by USO-g-gauze in pig femoral vein injury model.

Supplementary References

1. Pertile, R.A.N., Andrade, F.K., Alves, C. & Gama, M. Surface modification of bacterial cellulose by nitrogen-containing plasma for improved interaction with cells. *Carbohydr. Polym.* **82**, 692-698 (2010).
2. Sun, X. et al. Chitosan/kaolin composite porous microspheres with high hemostatic efficacy. *Carbohydr. Polym.* **177**, 135-143 (2017).
3. Anitha, A. et al. Chitin and chitosan in selected biomedical applications. *Prog. Polym. Sci.* **39**, 1644-1667 (2014).
4. Perdew, J., Burke, K. & Ernzerhof, M. Generalized gradient approximation made simple. *Phys. Rev. Lett.* **77**, 3865-3868 (1996).
5. Grimme, S. Semiempirical gga-type density functional constructed with a long-range dispersion correction. *J. Comput. Chem.* **27**, 1787-1799 (2006).
6. Wu, X., Vargas, M., Nayak, S., Lotrich, V. & Scoles, G. Towards extending the applicability of density functional theory to weakly bound systems. *J. Chem. Phys.* **115**, 8748-8757 (2001).
7. Kresse, G. & Hafner, J. Ab initio molecular dynamics for liquid metals. *Phys. Rev. B* **47**, 558-561 (1993).
8. Kresse, G. & Hafner, J. Ab-Initio molecular-dynamics simulation of the liquid-metal amorphous-semiconductor transition in germanium. *Phys. Rev. B* **49**, 14251-14269 (1994).
9. Blochl, P. Projector augmented-wave method. *Phys. Rev. B* **50**, 17953-17979 (1994).
10. Li, W. & Neuhauser, D. Real-space orthogonal projector-augmented-wave method. *Phys. Rev. B* **102**, 195118 (2020).
11. Gessler, K. et al. β-D-Cellotetraose hemihydrate as a structural model for cellulose II. An X-ray diffraction study. *J. Am. Chem. Soc.* **117**, 11397-11406 (1995).